13th ewtec 2019 Proceedings of the 13th European Wave and Tidal Energy Conference 1-6 Sept 2019, Naples, Italy

Motion tracking of a free-yawing floating tidal stream turbine platform

Thomas Lake, Alison Williams, and Ian Masters

***Abstract*—As part of ongoing work to develop and validate a combined model for the behaviour and potential power generation of a floating tidal energy converter, the motion of a prototype device has been recorded over a two month testing period. The inputs from several types of sensor have been combined with GPS position information to improve accuracy of the reported position, and the distribution of this position and orientation under different operating conditions is illustrated and discussed. The position distribution is consistent with other published work describing the motion of this platform. Further work will improve the processing of the underlying data and extend the model to take advantage of the redundant information available.**

***Index Terms*—Tidal Energy, Motion tracking, Data acquisition**

I. Introduction

RECENT years have seen a range of floating tidal energy converters (FTECs) deployed as part of the still growing marine energy sector. These devices are effectively a combination of a floating structure (a subject on which there is a great deal of existing expertise, regulation and understanding) and a tidal energy converter - a category of device which is still under rapid and active development, but for which there is also a good deal of existing information.

Investigating and identifying the combined response of these FTECs to varying and extreme environmental loads can help determine some of the ways in which both the capital and operating expenditure required can be reduced. The response of the device under loads can also inform predictions of how the device may be affected by fatigue, with associated implications for design life and therefore design criteria for new devices.

Swansea University is part of the SURFTEC project (**Su**stainability and **R**eliability of **F**loating **T**idal **E**nergy **C**onverters), investigating the measurement, prediction and implications of the loads on this class of tidal energy device. The first two work packages on this project include updating and adapting an in-house blade element momentum theory (BEMT) code and coupling this to a floating body model, and collecting and analysing data from PLAT-I - a prototype FTEC designed and operated by Sustainable Marine Energy (SME) [1].

The data collected and analysed from this platform will then be used to validated the outputs of the coupled BEMT and floating body model, before using that model to investigate possible loadings on a generic device under a range of environmental conditions and operating scenarios.

This paper aims to illustrate how Kalman filtering can be used to combine recorded position and sensor data to reconstruct the motion and orientation of a floating tidal device.

II. Equipment design and specifications

In order to validate the coupled BEMT and floating body model, it is necessary to record the motion of the platform alongside its operating condition, generated power and the incident flow onto the turbines. The operating condition, inlet flow and the device geometry can be provided to the coupled model as input data, with the output of the model compared to the recorded motion and generated power results.

After some preliminary investigation and testing, it was not possible to find a commercial off-the-shelf (COTS) system that was able to record the desired data while also meeting other design constraints, so a combined system was designed based on a combination of commercial and in-house components.

This system consists of a core data logging component, two custom sensor inertial measurement units and a single board computer providing additional logging, supervision and remote access to the system.

A. Core logger

The core logging component of the SURFTEC system is a Race Technology DL1 Pro, which incorporates a GPS receiver (providing position and velocity data), 3-axis accelerometer and supports logging external data provided digitally via two serial inputs as well as external analog inputs for voltage based sensors [2].

This unit can be monitored and controlled over a USB connection, as well as logging directly to SD Card. Due to the volume of data being recorded it was not possible to monitor all data over USB, leading to two separate streams of data – a high sample rate set stored on the SD card and a lower sample rate set recorded by the control computer over the USB connection. This provided some level of redundancy in case of storage media failure or if the SD card capacity was reached.

Paper 1328, Tidal device development and testing
This work was supported in part by the EPSRC under grant EP/N02057X/1

All authors are part of the Marine Energy Research Group, College of Engineering, Swansea University, Bay Campus, Fabian Way, Swansea, SA1 8EN.
The authors' email addresses are t.lake@swansea.ac.uk, alison.j.williams@swansea.ac.uk and i.masters@swansea.ac.uk respectively.

B. Inertial Measurement Unit (IMU)

Supplementing the accelerometers and GPS receiver in the core logger, a pair of remote sensor units were designed and built. Each unit is designed to be robust, waterproof and with the option to reprogram in the field if required.

Each unit consists of an Arduino Micro and two LSM9DS0 iNEMO inertial modules on a breakout board. The inertial modules combine a 3-axis accelerometer, 3-axis gyroscope and 3-axis magnetometer into a single package, along with a temperature sensor. The sensors can be configured to either return data across a wide measurement range (at lower precision) or across a smaller measurement range at greater precision. As an example, the accelerometer can be configured to report values between ± 2g with a precision of 6.1×10^{-5}g or between ± 16g with a precision of 7.3×10^{-4}g. Similar options exist for both the magnetometer and gyroscope portions of the sensor.

In each IMU unit, the two inertial modules are configured with different measurement ranges to take advantage of this option to allow a more precise measurement of values in the general case while also allowing larger peak values to be recorded in the case of a more extreme event. The use of two sensors also provide for a level of redundancy in case of failures

The two IMU units also include supporting circuitry to allow the units to be powered from a range of input voltages and to convert the output data signalling from TTL logic level communication to RS-485 differential serial signalling. This signalling standard was chosen in order to provide more robust data transfer between the sensor units and the core logger in the possibly noisy electrical environment of a power generating platform.

C. Control, supervision and remote access

One of the design requirements of the data logging system is that it needed to be able to operate with as little on site interaction as possible. This was implemented by planning enough storage space to exceed the planned deployment duration and placing a single board computer within the equipment case to provide remote access. The core logger was connected to this single board computer, allowing data from the core logger to be recorded and for the limited remote control of the logger. The data streamed from the logger to the PC stores data at a lower sample rate (25Hz) than the data saved to the SD card in the core logger (which records at 85Hz).

To allow remote access without requiring extensive configuration changes to be made to the networking on the platform, the computer established two SSH tunnels at boot, connecting to a server running on Amazon Web Services and to a desktop machine at Swansea University. This allowed two routes of access in case of misconfiguration or network difficulty, while allowing larger file transfers to avoid transiting through the Amazon network (and subsequent bandwidth costs).

The control PC and core logger were contained in a single equipment case along with DC-DC power supplies to supply 5VDC and 12VDC to the PC, logger and RS-485 interfaces. The RS-485 interface boards converted the signal from the sensor units to standard RS-232 TTL signal that could be decoded by the core logger.

For the first deployment of the logging equipment, this control computer was a Raspberry Pi 3B, with additional flash memory to provide storage. The Raspberry Pi was found to be operating very close to the limit of its input/output capacity at various points during this initial deployment, and has been replaced with an ODROID XU-4 computer and solid state drive for the second deployment (not presented here), providing more capacity and computing power.

D. ADV Integration

The data logging system also incorporates data from a Nortek Vector acoustic doppler velocimeter (ADV) running in continuous sampling mode, with the data recorded by the control PC. The maximum sample rate of 64Hz was used. Due to the planned deployment length the internal power supply and storage of the ADV were not used. The recording process was automatically stopped and restarted briefly at midnight UTC each day in order to resynchronise the ADV clock with the control PC and minimise drift.

III. Deployment

E. PLAT-I

PLAT-I is a floating tidal energy converter designed and under test by Sustainable Marine Energy. The platform is "a three-hulled tidal energy platform" [3], capable of freely rotating with the dominant flow direction. The platform hosts 4 SCHOTTEL instream turbines (SITs), for a total generating capacity of 280kW [3]. This initial version of the platform is not grid-connected, with generated energy being transferred into a load bank immersed off one side of the central hull.

Fig. 1. PLAT-I on location at Connel (Photo by T.Lake)

The platform, shown in fig. 1, has three hulls joined by a cross-deck structure towards the rear of the platform. The locations of key equipment are indicated in fig. 2. The two IMUs were installed under this cross deck structure towards the outboard ends, with the

core logging equipment installed inside the shipping container on the central hull. The GPS antenna was attached to one of the standoffs securing the shipping container to the central hull, at the position indicated on the diagram. Other instrumentation installed by SME is not included in the figure.

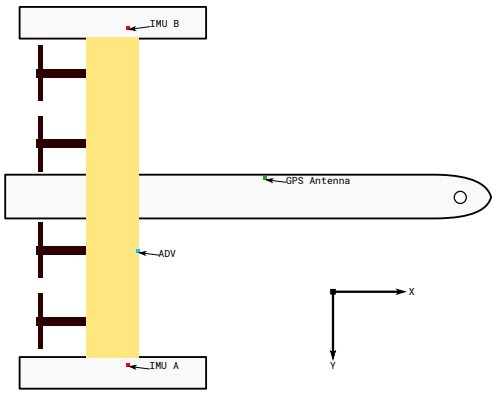

Fig. 2. Simplified top view of PLAT-I showing key instrument positions

F. Trial site: Connel, Scotland

The initial trial deployment was carried out south west of the Falls of Lora at Connel, Argyll and Bute, Scotland [4]. The site is relatively sheltered from waves, but has a pronounced ebb-flood asymmetry. This asymmetry is due to constrained flow of water entering and leaving Loch Etive through a shallow, narrow neck under Connel bridge. The shallow depth at the bridge creates underwater overfalls on the ebb tide which lead to a pronounced jet to the west of the bridge on the ebb tide [3], [4]. This jet leads to a faster but more variable flow past the platform on the ebb side of the tide.

Based on the ADV data recorded, the average flow speed at the platform over a flood tide was 0.20ms^{-1} and 1.20ms^{-1} during ebbs. The average of the peak velocities for flood and ebb respectively were 0.58ms^{-1} and 2.37ms^{-1}.

G. Recorded data

Testing took place between November 2017 and June 2018, with principal data collection for the SURFTEC project taking place in December 2017 and January 2018. Due to some equipment failures during the deployment, some data was lost or not recorded. In total, 744 hours of data were recorded at the highest sample rate available, with a further 371 hours of data recorded with full rate ADV data but only the lower sample rate stream of motion data. There were 373 hours during this period where no data was recorded or usable.

IV. Processing and Analysis

A combined dataset was created using higher rate IMU and GPS data where available, with gaps in the higher rate record being filled with lower rate data. An example of data from one of the sensors in this dataset is shown in fig. 3.

The data available from the IMUs gives information about the linear acceleration (from the accelerometers), angular velocity (from the gyros) and orientation (from the magnetometers). These sensors are imperfect, and are subject to noise, bias and interference from external sources. The GPS data returns position information, but is also subject to error (although an estimate of this error is also returned). It is, however, possible to combine data from all of these sources to compute a best estimate of the actual value of each parameter. This can be carried out using Kalman filters [5], which are frequently used to address this class of problem.

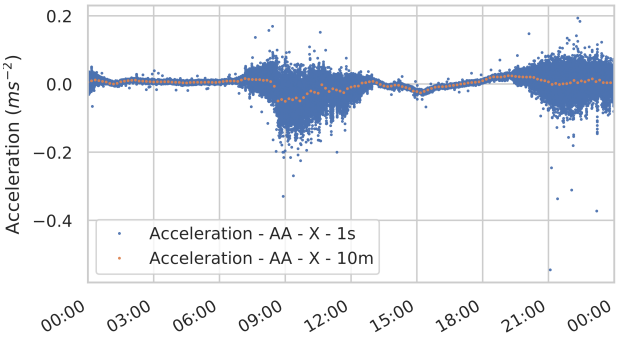

Fig. 3. Example timeseries showing x-axis acceleration from unit A, sensor A for 1 second and 10 minute averages over a 24 hour period. Axes as per fig. 2

H. Kalman filtering

Kalman filtering is an iterative process comparing a modelled internal state of a system to a set of measurements of that system. The process takes the internal state at a given time, predicts the state at the next timestep based on the internal physics imposed on the model and compares this prediction to measured values. Kalman filters can be applied to a range of linear problems, provided that the model used to predict the behaviour of the system is sufficiently described. Tracking the motion of a device by fusing together information from a number of sensors is a popular use of a Kalman filter [6].

A basic Kalman filter operates as follows [7]:

1) Initialise filter with an initial state $\vec{x}$ and 'belief' in that state, $\boldsymbol{P}$
2) Make a prediction for the state of the system at time $t + \delta t$ using the transition matrix, $\boldsymbol{F}$
   - Because the prediction is uncertain, update $\boldsymbol{P}$ to reflect this
3) Get a measurement of the system ($\vec{z}$ and belief in that measurement, $\boldsymbol{R}$)
4) Compute the difference between the predicted and measured states
   - Use this to compute a scaling factor to select whether the prediction or measurement is most reliable
5) Set new state to a combination of the predicted and measured values using scaling factor
6) Update the 'belief' in this new state using the scaling factor

7) Go to 2 and make new prediction

In this document, the notation and symbols correspond to those in [7]. The 'belief' in the state of the system or in the accuracy of the measurements provided is more mathematically described as the variance (and co-variance) of the relevant variables. The predictions of how the system moves from one state at t to another at $t + \delta t$ are encoded in the transition matrix $\boldsymbol{F}$.

The uncertainty in the prediction in step 2 is represented mathematically by a $\boldsymbol{Q}$, the 'process noise' [7] or 'covariance of random excitation' [5]. This represents any unmodelled effects that aren't included in the transition matrix, or which aren't represented in the state variables. An example of this would be higher order effects neglected in a simple model - e.g. accelerations in a constant velocity model.

I. A simplified motion model

To start the analysis of the motion data captured on PLAT-I, a simplified model was constructed around three degrees of freedom. The three degrees of freedom represented are global position (E, N) and heading (ψ). The model also tracks the first and second time derivatives of each of these degrees of freedom - i.e. velocity and acceleration. The accelerations are assumed to remain constant throughout each timestep (i.e. the third time derivative of each degree of freedom is zero). This model was implemented in Python, using the filterpy library from [7] as the basis.

The position of the platform is represented as UTM coordinates in zone 30V, with the heading representing rotation clockwise from north. The sensor values returned from the device are all reported in a local coordinate frame, and must be converted to equivalent values in the global frame based on the current heading of the device.

The transition between each timestep is calculated as:

$$d = d + \dot{d}\delta t + \frac{1}{2}\ddot{d}\delta t^2 \tag{1}$$

$$\dot{d} = \dot{d} + \ddot{d}\delta t \tag{2}$$

$$\ddot{d} = \ddot{d} \tag{3}$$

for each degree of freedom, $d \in E, N, \psi$.

These equations are written in matrix form for each degree of freedom to create the transition marix, $\boldsymbol{F}$ referenced above. Additionally, the value of ψ at the end of each timestep is checked, and if found to lie outside the range $[-\pi, +\pi]$ it is converted to an equivalent value within the range.

The duration of each timestep (represented as δt above) is determined from the provided input data.

The measurements provided to the filter at each timestep include the reported GPS position and accuracy, the magnetic heading (with some caveats discussed later) and reported angular velocity about the vertical axis of the device - equivalent to the rate of change of heading. In the results presented here, only one sensor from one IMU is included.

The initial state of the filter is set to the first measurement from the recorded data used, with relatively large variances set in $\boldsymbol{P}$ to reduce run-in time. For each subsequent set of measurements input to the filter, the associated belief $\boldsymbol{R}$ in the measurements is updated with the reported accuracy (for GPS position data), or based on values in the sensor datasheet.

An example of the output of this model is shown in fig. 4, showing the positions output by the filter alongside the corresponding input GPS data for a 30 minute period with the platform operational. The colour of each marker in fig. 4b is mapped to the sum of the variances for the two coordinates and the GPS data shown in fig. 4a is coloured by the square of the reported accuracy, to allow comparison on the same scale as the modelled data. The range of the colour

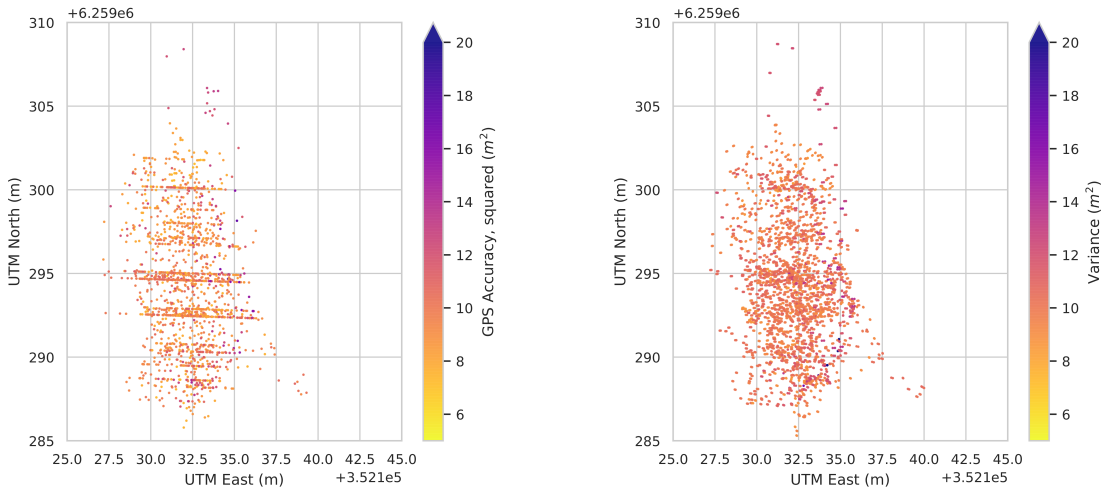

(a) GPS input

(b) Model output

Fig. 4. GPS position data and model output, showing position over a 30 minute period. Points coloured by reported accuracy squared (GPS) or variance (model) respectively

map has been clipped to highlight variations in a larger selection of points.

Comparing the input GPS data shown in fig. 4a to the output of the model in fig. 4b shows that the motion here has been smoothed, with some of the horizontal banding evident in the input GPS data removed.

J. Sensor drift, interference and calibration difficulties

One of the disadvantages of low cost MEMS devices is that the outputs can be noisy, and prone to drift over longer periods. Some of this is handled by the Kalman filtering process - drift in the accelerometers can be compensated for by the GPS position, and drift in the gyros can be compensated for by the magnetometers. Any change in the behaviour of the magnetometers, however, cannot be corrected for in this manner.

This is compounded by the difficulty in calibrating the magnetometers during the initial fitting. (While rotating the box on all axes in close proximity to its fitted position is a simple enough procedure in theory, it is somewhat harder to do while providing reliable power and data connections on a partially assembled tidal platform!)

As described in [8], the magnitude of the external magnetic field acting on the sensor at a given location is effectively constant, allowing the magnetometer data to be normalised by fitting the returned values to an ellipsoid and using this fit to transform the data to lie on a unit sphere centered at the origin. Orientation data can then be obtained using trigonometry and then fed into the Kalman process.

Fig. 6 shows both raw and corrected magnetometer readings. As the figure illustrates, the rotation of PLAT-I about it's mooring ensures that the magnetometer data covers enough of an ellipse in the x,y plane to be fit reasonably. While this allows the device heading to be recovered, the lack of significant pitch and roll motion makes it harder to apply this method in those axes - although the smaller motion in pitch and roll is understood to be a good design feature in any other respect!

In addition to the effect of the metal surrounding the IMUs and the drift of sensors over time, additional interference was observed in the magnetometer readings due to the use of a winch located near to the IMU

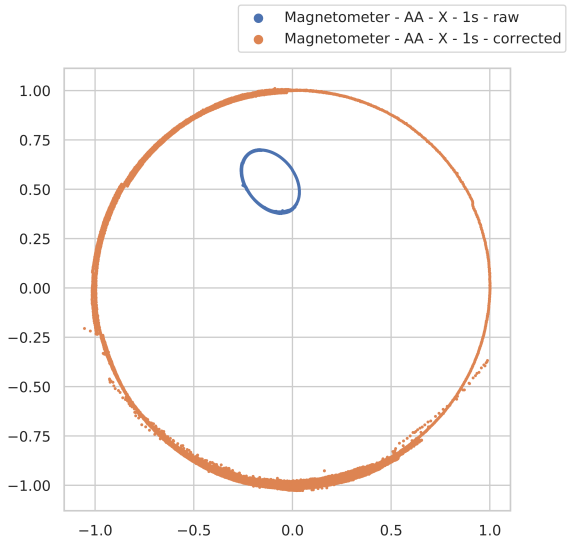

Fig. 6. Plots of the X,Y magnetometer readings pre- and post-rescaling

units. The brief periods where this equipment appears to have been in use have been excluded from analysis, with the magnetometer rescaled using the ellipse fitting method described above after the excluded data.

V. Results

During the testing conducted at Connel, PLAT-I can be described as being in one of three states, as discussed in [4]. These states are:

a) Operational - generating power
b) Rotors parked - turbines in the water, but stationary
c) SDMs[1] raised - turbines raised out of the water

The recorded data has been classified into each of these three states, and each contiguous period filtered using the Kalman filtering process described abov, using the one second mean values of the underlying data as input. The one second mean values were used in this instance to ensure a consistent timestep, and to reduce the computational cost of this initial investigation.

[1]SDM: SIT deployment module - a moveable arm connecting each SIT to the platform

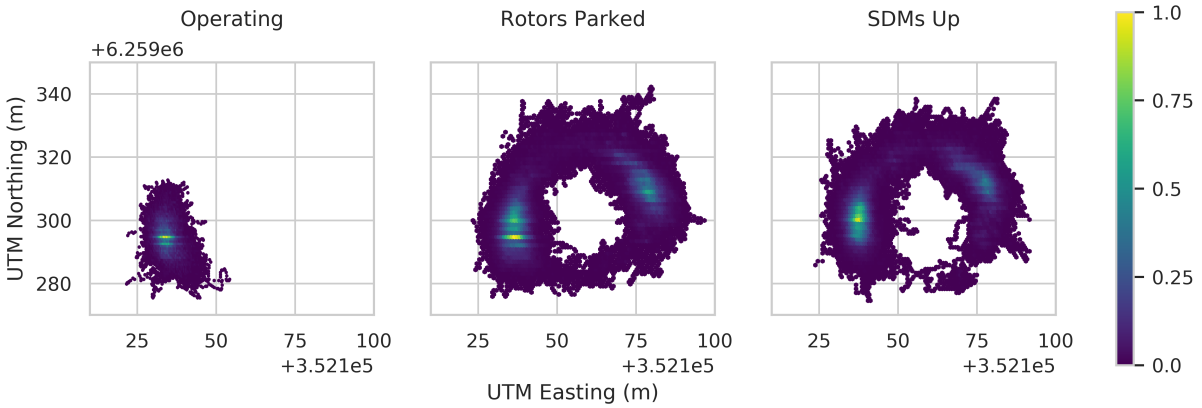

Fig. 5. Distribution of modelled position for operating, rotors parked and SDMs raised conditions

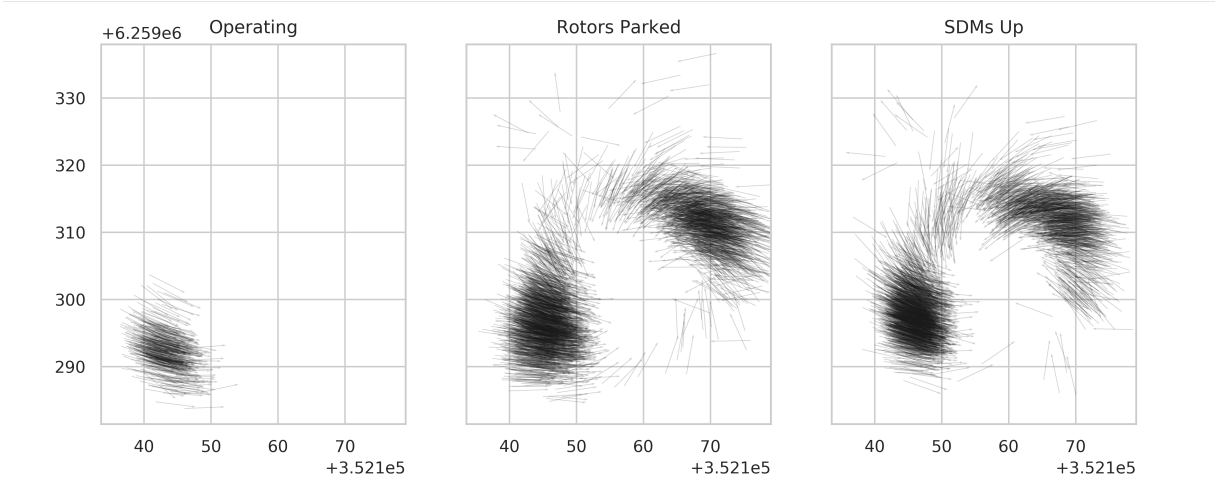

Fig. 7. Platform position and orientation, based on two minute mean values

The distribution of positions for each state are shown in fig. 5, represented as hexagonal bins coloured by the number of samples in each bin. As the total time the platform was recorded in each of the three operational states varies (with the operating state being the smallest dataset), the colour range in each plot has been normalised against the duration of the input data.

It should be noted that for both the raw GPS data and the model results, the reported position is the location of the SURFTEC GPS antenna, shown relative to the rest of the device in fig. 2. This is why these results differ from the positions reported in [4], although the trends illustrated are similar.

K. Operational

The distribution of positions for the turbines operating state is the smallest of the three cases, as generation only occurred on the ebb tide. The distribution shown in fig. 5 is based on generating periods from the ebb tide on three successive days. The resulting position data is spread around a central dominant location, with most points confined within the region extending approximately 15m north and 15m south east of the mean. This would be consistent with PLAT-I rotating about the mooring turret during operation, but primarily located around the mean flow direction as discussed in [4].

This is also reflected in the yaw data in the model, with the reported heading varying over a $160°$ range, with a standard deviation of $8.6°$ based on the 1Hz input data. This distribution reduces to a range of $51°$ and a standard deviation of $6.7°$ when averaged over two minute intervals. The two minute average values of platform position have been used to generate the plots shown in fig. 7, with the head of the arrows representing the approximate location of the bow of the platform.

L. Rotors Parked

Comparing the distribution of position with the rotors parked (fig. 5) to the distribution for the operational state, the most immediate difference is that the distribution forms an ellipse around a central point - this shows the rotation of the platform about the turret, with an approximately 14m radius between the turret and the GPS antenna position being reported here.

The distribution has two distinct higher density regions - one to the south west in a similar location to the operational case, and one to the north east, almost but not quite diametrically opposite. These regions represent the dominant position during ebb and flood phases of the tide respectively. The distribution shows more occupied bins to the north than the south, which is consistent with the platform rotating more often to the north of its moorings when transitioning during the changing tides. The higher density region associated with ebb tides is slightly larger than the corresponding region in the operating case - it is likely that the lower thrust in the parked state allows the platform to more easily move in the lateral direction.

The motion model estimates position and heading, but there is no assumption imposed that these are correlated. However, we observe that the platform heading does appear to be correlated with position in a manner consistent with the both position and heading depending on the dominant flow direction and mooring design. As could be expected from the position plots, the range of headings recorded with the rotors parked covers the full range from $0°$ to $360°$.

The region to the south west of the reported positions shown for parked rotors in fig 7 shows a predominantly easterly heading, with the region to the north east showing a predominantly westerly heading, reflecting the approximate flow directions for the ebb and flood respectively. It can be seen that a cluster of values toward the north west of the rotors parked plot in fig. 7 appear to be pointing away from centre - this seems improbable based on the platform position and mooring design and appears to be an artefact of the averaging process. This requires further investigation.

M. SDMs Raised

The last case represents a maintenance state, with the turbines raised out of the water. This reduces the drag on the platform, and examination of the position data presented in [4] shows larger deviations from

the mooring centre in this case due to this reduction. Comparing the higher density region associated with ebb flows to the equivalent region in the operating and parked cases, is slightly further north, with a narrower east-west distribution and larger north-south spread. This would be consistent with the increased range of motion discussed in [4]. The whole distribution is also narrow in the east-west axis, which would be consistent with the reduced drag placing less load on the moorings and allowing the platform to sit closer to the centre.

The platform orientation data for this case provides a very similar plot to that for the rotor parked case. Numerically, the range of headings reported based on two minute average values is smaller than in the rotors parked case ($295°$ compared to $352°$)- largely due to the reduced presence of the platform towards the south of the area.

VI. Conclusions

The work shown here illustrates that a Kalman filter can be used to combine recorded position and motion data and reconstruct the motion and orientation of a floating tidal device. Some of the challenges that can arise when dealing with sensors over a longer duration deployment and methods for recalibrating magnetometer data in post processing have also been shown. Despite this, the results presented are consistent with existing published work and the expected behaviour of the platform and provide a solid basis for future development and analysis.

Following from this work, it is intended to extend the filter to account for full three dimensional movement. This will require the magnetometer data to be fit and transformed onto a sphere rather than a circle (to give a pitch and roll reference), and for the remaining data in other sensor axes to be incorporated.

The model should also be extended to incorporate the remaining sensors and take advantage of the redundancy this gives. There are a number of approaches that can be taken here, but they can include either the use of multiple Kalman filters to process each input to the model (i.e. Filter all x-axis acceleration to give a single reading input into the motion model) or to run the full motion model in parallel with some filtering of the resultant data.

Since collecting the data used in this paper, PLAT-I has been re-deployed at Grand Passage, Nova Scotia. Further work will also include applying the model presented here to the data collected in this second deployment.

Acknowledgement

The authors would like to thank Sustainable Marine Energy for allowing the use of their platform to collect the data presented here, and their ongoing support with future work.

References

[1] Sustainable Marine Energy. [Online]. Available: https://sustainablemarine.com/

[2] Race Technology Ltd. (2015) DL1 PRO/WP and DL2 Introduction. [Online]. Available: https://www.race-technology.com/wiki/index.php/DL1PRO-WP/Introduction

[3] R. Starzmann, I. Goebel, and P. Jeffcoate, "Field performance testing of a floating tidal energy platform - part 1: Power performance," in *Asian Wave and Tidal Energy Conference*, 2018. [Online]. Available: https://www.researchgate.net/publication/326572960_Field_Performance_Testing_of_a_Floating_Tidal_Energy_Platform-Part_1_Power_Performance

[4] P. Jeffcoate and N. Cresswell, "Field performance testing of a floating tidal energy platform - part 2: Load performance," in *Asian Wave and Tidal Energy Conference*, 2018. [Online]. Available: https://www.researchgate.net/publication/326573036_Field_Performance_Testing_of_a_Floating_Tidal_Energy_Platform-Part_2_Load_Performance

[5] R. E. Kalman, "A new approach to linear filtering and prediction problems," *Journal of Basic Engineering*, vol. 82, no. 1, p. 35, 1960.

[6] L. Drolet, F. Michaud, and J. Cote, "Adaptable sensor fusion using multiple kalman filters," in *Proceedings. 2000 IEEE/RSJ International Conference on Intelligent Robots and Systems (IROS 2000) (Cat. No.00CH37113)*. IEEE, 2000.

[7] R. Labbe. (2018) Kalman and Bayesian Filters in Python. [Online]. Available: https://github.com/rlabbe/Kalman-and-Bayesian-Filters-in-Python/tree/e84f8018366438c87189ccad40a56bf506f81ffc

[8] M. Kok, J. D. Hol, T. B. Schön, F. Gustafsson, and H. Luinge, "Calibration of a magnetometer in combination with inertial sensors," in *15th International Conference on Information Fusion*, pp. 787–793.